Article:
Shaukat, F., Raja, G., Gooya, A. et al. (1 more author) (2017) Fully automatic and accurate detection of lung nodules in CT images using a hybrid feature set. Medical Physics, 44 (7). pp. 3615-3629. ISSN 0094-2405

https://doi.org/10.1002/mp.12273

Fully automatic and accurate detection of lung nodules in CT images using a hybrid feature set

Furqan Shaukat[a,b,*] , Gulistan Raja[b], Ali Gooya[a], Alejandro F. Frangi[a]

[a]*Department of Electronic and Electrical Engineering, University of Sheffield, Mappin Street, Sheffield S1 3JD ,UK.*
[b]*Department of Electrical Engineering, University of Engineering & Technology, Taxila 47080, Pakistan.*

Purpose: The aim of this study was to develop a novel technique for lung nodule detection using an optimized feature set. This feature set has been achieved after rigorous experimentation, which has helped in reducing the false positives significantly.

Method: The proposed method starts with pre-processing, removing any present noise from input images, followed by lung segmentation using optimal thresholding. Then the image is enhanced using multi scale dot enhancement filtering prior to nodule detection and feature extraction. Finally, classification of lung nodules is achieved using Support Vector Machine (SVM) classifier. The feature set consists of intensity, shape (2D and 3D) and texture features, which have been selected to optimize the sensitivity and reduce false positives. In addition to SVM, some other supervised classifiers like K-Nearest-Neighbour (KNN), Decision Tree and Linear Discriminant Analysis (LDA) have also been used for performance comparison. The extracted features have also been compared class-wise to determine the most relevant features for lung nodule detection. The proposed system has been evaluated using 850 scans from Lung Image Database Consortium (LIDC) dataset and k-fold cross validation scheme.

Results: The overall sensitivity has been improved compared to the previous methods and false positives per scan have been reduced significantly. The achieved sensitivities at detection and classification stages are 94.20 % and 98.15 % respectively with only 2.19 false positives per scan.

Conclusions: It is very difficult to achieve high performance metrics using only a single feature class therefore hybrid approach in feature selection remains a better choice. Choosing right set of features can improve the overall accuracy of the system by improving the sensitivity and reducing false positives.

Keywords: CAD, Feature extraction, Lung nodule detection.

1. INTRODUCTION

Lung cancer is one of the leading causes of the deaths around the world with the smallest rate of survival after diagnosis. The survival rate can be increased by early nodule detection.[1] Lung cancer is found in both developed and under developed countries.[2] The current five-year survival rate is only 16%, [3,4] and estimates suggest that by 2030, lung cancer will reach around 10 million deaths per year.[2]

* Corresponding author. Tel.: +0-092-333-5903313. Fax: +0-092-543-602003.
E-mail addresses: f.shaukat@sheffield.ac.uk, furqan.shoukat@uettaxila.edu.pk (F. Shaukat), gulistan. raja@uettaxila.edu.pk (G. Raja), a.gooya@sheffield.ac.uk (A. Gooya), a.frangi@sheffield.ac.uk (A. Frangi).

The main reason for lung cancer is the formation of cancerous nodules in lung lobes or lung periphery. Nodules can be defined as lung tissue abnormalities having a roughly spherical structure and diameter of up to 30 mm.[3,4] They can be classified into the following categories: well-circumscribed, juxta-vascular, juxta-pleural, and pleural tail. Well-circumscribed nodules are solitary nodules having no attachment to their neighboring vessels and other anatomical structures. Juxta-vascular nodules show strong attachment to their nearby vessels. Juxta-pleural nodules are found to have some attached portion to the nearby pleural surface. Pleural tail nodules, having a tail which belongs to the nodule itself, show minute attachments to nearby pleural wall.[5] Sample images of different nodule groups can be seen in Fig. 1.

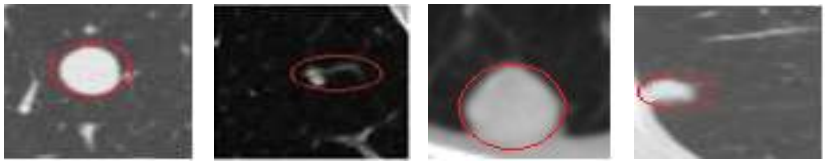

Fig. 1. Sample images of four nodule groups. From left to right, well-circumscribed, juxta-vascular, juxta-pleural and pleural tail nodules.

Computer Aided Detection (CAD) can play an important role in aiding early detection of the cancer.[6] Because of their rapid growth and increasing reliability of medical imaging technologies, CAD systems are critical for objective diagnosis and timely early detection. The main idea of a CAD system is the extraction with high accuracy of the region of interest (ROI) imaged through CT, PET, MRI or other imaging modalities.[7-9] A complete diagram for the lung CAD process, suggested in this paper, is shown in Fig. 2. The steps involved in this process are briefly explained below.

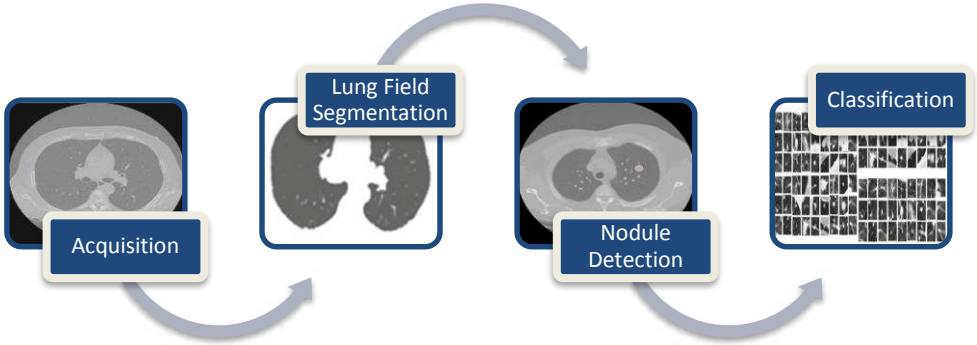

Fig. 2. Process of lung nodule detection consists of acquiring an image followed by lung segmentation, nodule detection and false positive reduction or classification.

Image acquisition can be defined as a process of acquiring medical images from imaging modalities.[4] Many common methods are available for lung imaging. Computed Tomography (CT) stands out as a key imaging modality compared to other lung imaging methods for the primary analysis of lung nodules screening. The Lung Image Database Consortium (LIDC), [10] stands out among the available public databases due to the standard

radiological annotations provided with the images and its widespread use. Others databases are, Early Lung Cancer Action Program (ELCAP) Public Lung Image Database, [11] and ELCAP Public Lung Database to Address Drug Response.[12]

Lung segmentation can be defined as the process of extracting the lung volume form input CT image and removing the background and other irrelevant components. Lung segmentation serves as a prerequisite to the nodule detection. Accurate lung segmentation plays an important role to enhance the efficiency of lung nodule detection system. Numerous methods have been proposed in literature for the extraction of lung volume from CT image such as optimal thresholding, rule-based region growing, global thresholding, 3-D-adaptive fuzzy thresholding, hybrid segmentation, and connected component labeling. After the initial segmentation, juxta-pleural nodules are included by refining the extracted lung volume. To do this, a chain-code method, a rolling ball algorithm, and morphological approaches have been generally used.[13-22]

Nodule detection can be defined as the process of detecting suspicious areas in lung lobes which may cause the lung cancer. It is performed after lung segmentation which decreases the workload by removing the background and unwanted areas from input CT image. Various methods have been presented in the literature for lung nodule candidate detection. Multiple gray-level thresholding stands out among available methods. Moreover, shape-based, template-matching-based, morphological approaches with convexity models and filtering-based methods have been used for this purpose.[13-17, 23-24]

After nodule candidate detection, we have to classify them into nodules and non-nodules. In literature, this step is commonly referred to as false positive reduction and it comprises of two steps (i) Feature Extraction (ii) Nodule Classification where nodule classification here means classification of nodule candidates into nodules and non-nodules. Several methods of extracting image features and nodule classification are proposed in literature. Most used features are intensity based statistical features, geometric features and gradient features.[13-14] With the help of extracted feature vectors, nodules are detected through various supervised and un-supervised classifiers with reduced amount of false positives.[15-17,19,25-27] We briefly review the related work in the following, highlighting the challenges which have motivated our work in this paper.

This section presents a group of papers which have used small datasets containing small number of nodules. It is presumable that the performance of the systems will be worsened in various more realistic scenarios with broader range of nodule types present in clinical scans. Cuenca *et al.*[16] proposed a CAD system for solitary pulmonary nodule detection in CT images using an iris filter. Lung volume was segmented using adaptive thresholding and features were extracted with the help of 3D iris filter. Linear Discriminant Analysis (LDA) was

applied to reduce the false positives (FP). The system achieved a sensitivity of 80% with 7.7 FP/scan. The system was evaluated using a private dataset containing only 77 solitary nodules, which are relatively easier to be detected. Guo *et al.* [28] proposed an adaptive lung nodule detection algorithm. The algorithm consisted of a feature selection and classification part. Eight features were selected after extraction and SVM was applied as a classifier. The system was evaluated using a private dataset of 29 scans with 2mm slice thickness including only 34 true nodules. Similarly, Sousa *et al.*[29] developed a method for automatic detection of lung nodules in CT images. They used subset of features to reduce the complexity and increase the speed of the system. Initially the system extracted 24 features and after selection, there were eight best features selected. The system obtained a FP/scan of 0.42 and 84.84% sensitivity. The dataset used to evaluate the system contains only 33 nodules (23 benign and 10 malignant). In the same manner, Liu *et al.*[30] presented a CAD based pulmonary nodule detection method based on analysis of enhanced voxel in 3D CT image. The method consists of multiple steps, including lung segmentation, candidate nodules enhancement, voxel feature-extraction and classification with Support Vector Machines (SVM). The system shows a good performance by achieving a sensitivity of 93.75% and 4.6 FP/scan but the dataset used consists of 32 cases containing only 33 solitary nodules. Next, Orozco *et al.*[31] proposed a novel approach of lung nodule classification in CT images without lung segmentation. Eight texture features from the histogram and the gray level co-occurrence matrix for each CT image were extracted. SVM was used for classification of nodule candidates into nodules and non-nodules after being trained with the extracted features. The reliability index of 84% was achieved. The system was tested using a private dataset consisting of only 38 scans with nodules. Tartar *et al.*[32] proposed a method for classification of pulmonary nodules by using different features. 2-D and 3-D geometrical and intensity based statistical features were used. The system achieved an accuracy of 90.7% and was evaluated using a private dataset consisting of 95 pulmonary nodules only.

A group of papers underperforms in terms of accuracy/sensitivity by having relatively lower accuracy/sensitivity as compared to other systems. Messay *et al.*[13] proposed a system for lung nodule detection in CT images. A set of 245 features were extracted and 40 were selected. The system was evaluated using LIDC dataset. Achieved sensitivity was 82.66% with 3FP/scan. The system detected nodules of juxta-vascular, juxta-pleural and solitary type, having sizes in the range of 3-30 mm. The system showed good performance in terms of FP/scan but underperforms in terms of sensitivity. Murphy *et al.*[33] proposed a CAD system using local image features and k-nearest-neighbor classification. The system was evaluated using a large private dataset, achieving sensitivity rate of 80% with 4.2 FP/scan. The system detected pleural and non-pleural nodules having size 2-14 mm using 813 scans. Retico *et al.*[34] proposed a fully automated system to detect the pleural nodules in low dose

CT-scan images. A feature set consisting of 12 texture and morphological features was extracted from each nodule candidate. The system achieved a sensitivity of 72% with 6 FP/scan. Teramoto *et al.*[35] proposed a hybrid method for the detection of pulmonary nodules using positron emission tomography/computed tomography. The proposed method was evaluated using 100 cases of PET/CT images. The system achieved a sensitivity of 83.0% with FP/scan of 5.0.

High false positive rate becomes a major issue in some other studies. Ozekes *et al.*[36] proposed a computerized lung nodule detection method using 3D feature extraction and learning based algorithms. The proposed system claimed sensitivity up to 100% and a false positive rate of 44 per scan. Moreover, system does not provide any information regarding the type of nodules in consideration. Assefa et al.[37] proposed a method based on template matching and multi-resolution for lung nodule detection. Seven statistical and two intensity based features were extracted for the false positive reduction stage. The system achieved an accuracy of 81% and a false positive rate 35.15%. Choi *et al.*[3] proposed a computer-aided detection method based on 3-D shape-based feature descriptor. A 3-D shape-based feature descriptor and a wall elimination method was introduced to include juxta-pleural nodules. The system was evaluated with LIDC images having 148 nodules. System achieved a sensitivity of 97.5% with 6.76 FP/scan.

Following section presents other studies highlighting some additional challenges. Mabrouk *et al.*[7] proposed a technique for automatic classification of lung nodules in CT images using two classifiers. A total of 22 image features were extracted. A fisher score ranking method was used as a feature selection method to select best ten features. The system showed good results while dealing with large nodules but failed to detect the smaller nodules. Choi *et al.*[9] proposed a detection method based on hierarchical block classification. The image was divided into sub blocks and an analysis was made on the basis of entropy and then sub blocks were selected having high entropy. System attained 95.28% sensitivity and 2.27 FP/scan only. The system shows a good performance overall but the system' ability to detect all types of nodules is limited. Tariq *et al.*[38] proposed a CAD system for pulmonary nodule detection in CT scan images using neuro-fuzzy classifier. A detailed feature set containing different properties were extracted and applied to neuro-fuzzy classifier. They claimed that the method is effective which can also detect small nodules. But the standard datasets and metrics to evaluate the system performance have not been discussed. In addition, system does not give any information regarding types of nodules in consideration. Akram *et al.*[39] proposed a SVM based classification of lungs nodule using hybrid features from CT images. The 2D and 3D geometric and intensity based statistical features were extracted and used to train the classifier. The sensitivity of 95.31% is claimed but the system does not give any information regarding FP/scan. In addition, the

number of nodules used to validate the results is too small. Hence, there is very little chance that the performance of the system will not be affected in various more realistic scenarios. The review of these CAD systems is summarized in Table 1.

Table 1 - Review of Current CAD Systems, *N/A means Not available.

CAD Systems	Data Set	No. Cases	No. Nodules	Extracted Features	Sensitivity (%)	FPR	Remarks
Cuenca *et al.* [16]	Private	22	77	Intensity, Morphological	80.00	7.70	
Guo *et al* .[28]	Private	29	34	Shape	94.77	N/A	
Sousa *et al.* [29]	Private	N/A	33	Shape, Texture, Gradient, Histogram, Spatial	84.84	0.42	Used dataset is too small containing less number of nodules.
Liu *et al.* [30]	Private	32	33	N/A	93.75	4.60	
Orozco *et al.* [31]	LIDC, ELCAP	128	75	Texture	84.00	7.00	
Tartar *et al.* [32]	Private	63	95	Shape	89.60	7.90	
Messay *et al.* [13]	LIDC	84	143	Shape, Intensity, Gradient.	82.66	3.00	Systems underperform in terms of sensitivity/ accuracy.
Murphy *et al.* [33]	Private	813	1518	Shape Index, Curvedness	80.00	4.20	
Retico et *al* .[34]	Private	42	102	Morphological, Texture	72.00	6.00	
Teramoto *et al.* [35]	Private	100	103	Shape, Intensity	83.00	5.00	
Ozekes *et al.* [36]	LIDC	11	11	Shape	100.00	44.00	High false positive rate make the schemes inefficient.
Assefa *et al.* [37]	ELCAP	50	165	Intensity, Statistical	81.00	35.15	
Choi *et al.* [3]	LIDC	84	148	Shape Based 3D Descriptor	97.50	6.76	
Mabrouk *et al.* [7]	Private	12	N/A	Shape, Intensity	97.00	2.00	System failed to detect smaller nodules.
Choi *et al.* [9]	LIDC	58	151	Shape, Intensity	95.28	2.27	System's ability to detect all type of nodules is limited.
Akram *et al.* [39]	LIDC	47	50	Shape, Intensity	95.31	N/A	System is evaluated with small number of nodules and FP/scan is not informed.

In summary, the review of the current schemes shows their lack of ability to detect all nodules while maintaining the same precision in terms of sensitivity and reduced number of false positives per scan. Most of the algorithms are optimized and limited to a particular set of data which limits the generalization of the results. In addition, the current schemes have not been evaluated on sufficiently large datasets to achieve more robustness. Therefore, methods evaluated having lesser number of nodules are not guaranteed to present the same performance in all

circumstances. Moreover, since feature extraction is very important for the characterization of the nodules from other anatomic structures present in the lung lobes, the choice of optimum feature set for nodule classification is still an unresolved issue. Thus the real challenge is to make more accurate systems in terms of sensitivity and reduced FP/scan with increased nodule diversity.

In this paper, we present a novel technique for pulmonary lung nodule detection using a set of optimum features and SVM classifier. An optimum feature set has been achieved after rigorous experimentation, which has helped in reducing the false positives significantly. Prior to nodule detection, an image enhancement technique has been used to increase the detection rate of low density nodules, which has helped to increase the sensitivity of the proposed system. A fully automated lung segmentation technique has been applied using optimal thresholding and connected component labeling. To the best of our knowledge no similar technique has been reported with the combination of steps that we have used. In addition to SVM, different classifiers have been used to evaluate the performance of the proposed system. Finally, an attempt has been made to determine the most relevant feature class in extracted feature set. The overall sensitivity has been improved compared to the previous methods and false positives per scan have been reduced significantly. The paper is organized as follows. Section 2 presents the proposed methodology for lung nodule detection. Section 3 presents the results and discussion and Section 4 presents the conclusion.

2. METHOD

The proposed methodology consists of series of steps which start with pre-processing followed by lung segmentation, image enhancement, nodule detection, feature extraction and classification of lung nodules. The block diagram of the proposed method is shown in Fig. 3. In preprocessing stage, the lung image is thresholded using optimal thresholding, then the background removal and hole filling operations are done on the image prior to lung segmentation from thresholded image. Contour correction is made to include juxta-pleural nodules using morphological operations. Before ROI extraction, i.e. identifying the candidate nodules, it is very important to make sure that all candidate nodules have been included. To this end, the contour corrected image is enhanced. The candidate nodules are detected and segmented simultaneously. Next, the features are extracted from lung nodule candidates and used for classification using SVM classifier.

2. A. Lung Segmentation

Lung segmentation has a critical importance as it is pre requisite to the nodule detection. Any in-accurate lung volume segmentation can lead to the low accuracy of whole system. In this paper we propose a fully automated

segmentation method for lung volume from CT scan images. For this purpose, we have used optimal thresholding followed by a connected component labeling and contour correction. For optimal thresholding, let T^i be the threshold after the i^{th} step. The lung CT scan can be divided in two density groups. The HU values in lung CT scan normally varies from -2000 HU to +2000 HU. The lung area also called non-body area is a low density area which ranges from -1000 HU to -500 HU. [39, 40] The CT scanner area is also part of the non-body area. The body area contains the surroundings of lung lobes. Because the lungs are in non-body area, we initially select a threshold value of -500 HU for T^o.

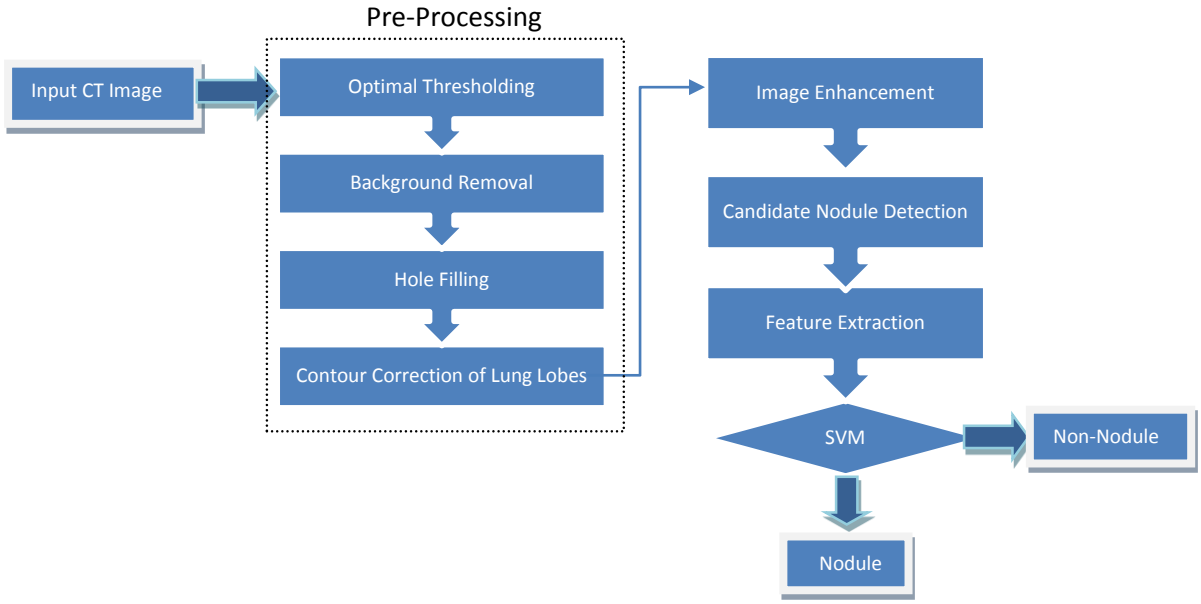

Fig. 3. Flow Chart of the Proposed Method.

For selection of new threshold, we apply T^i to the lung image. Let μ_o and μ_b be the mean intensities of the object and background in the lung region respectively, the new threshold is given by: [40]

$$T^{i+1} = \frac{\mu_o + \mu_b}{2} \tag{1}$$

In this manner this iterative approach carries on until our threshold converges to a point, and the optimal threshold T_{op} is obtained. As such, an initial segmented lung image volume $f(x, y, z)$ can be obtained as follows:

$$f(x,y,z) = \begin{cases} 1 & f(x,y,z) \geq T_{op} \\ 0 & f(x,y,z) < T_{op} \end{cases} \tag{2}$$

In which x and y indices represent the slice coordinates and z indicates the slice number. The volume consists of the total number of z slices and each slice has dimensions of $x \times y$ pixels. Results of optimal thresholding on a

few sample images can be seen in column (b) of Fig. 4. After applying optimal thresholding we get a lung CT image which contains body and non-body area. White area belongs to non-body area and black belongs to body area. We are interested in extracting the lung region from non-body voxels. To achieve this, we apply 3D connected component labeling to initially thresholded image $f(x, y, z)$ to acquire the lung region from non-body voxels. Using this technique the first and second largest volumes are selected. Most of the unwanted non-body components are ignored in the volume selection. After the background removal, the resultant image at this stage contains holes in lung lobes, which may be potential nodules or vessels. These must be included to the lung region for accurate detection and thus filled by morphological operations. The resultant image at this stage can be seen in column (c) of Fig. 4. The hole-filled image may contain the potential nodules at the border known as juxta-pleural nodules. To include these, we use a rolling ball algorithm.[41] Final process images are shown in column (e) of Fig. 4.

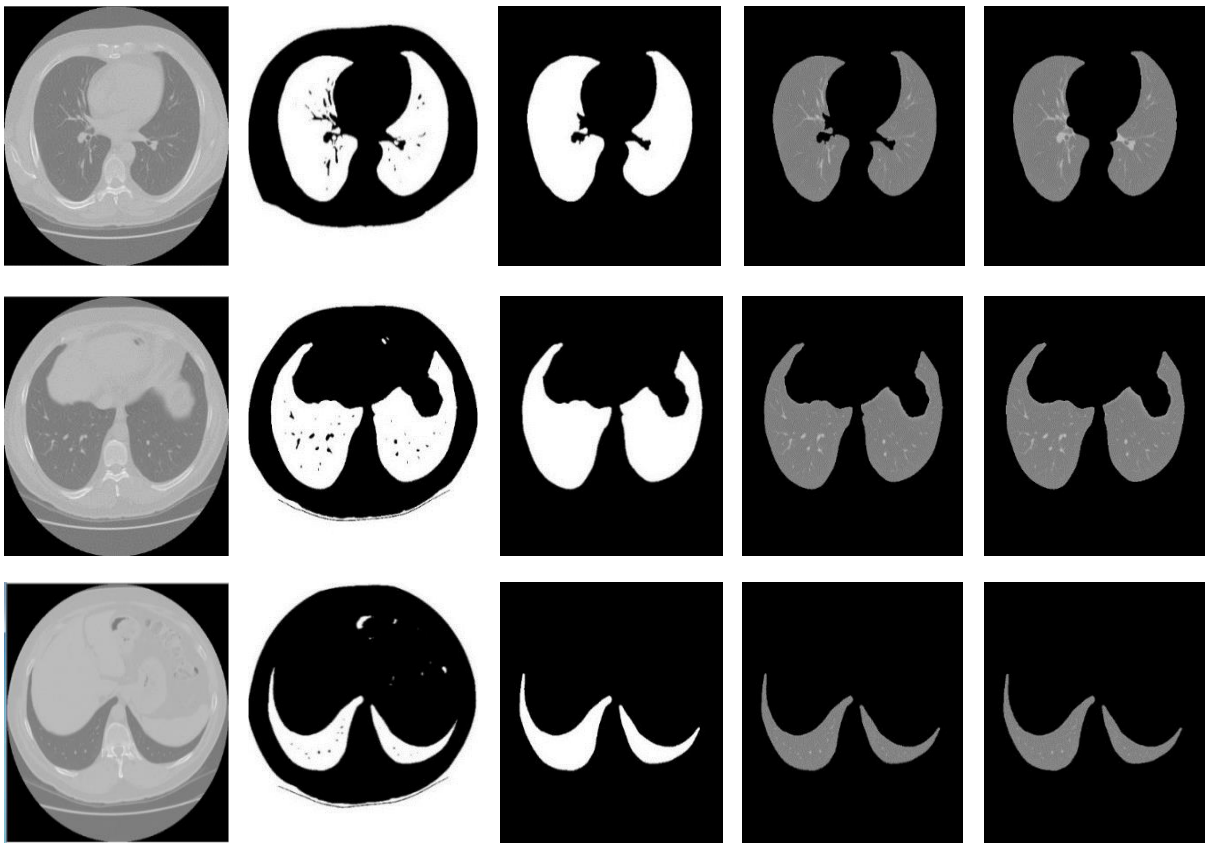

(a) (b) (c) (d) (e)

Fig. 4. Example images of lung volume segmentation, (a) to (e) from left to right presenting input, thresholded, hole filled, lung segmented and contour corrected images, respectively.

2. B. Image enhancement and nodule detection

Image enhancement is very critical for the sensitivity of the lung nodule detection system as it plays an important role in detection of the nodules by enhancing them and reducing false positives by weakening the other structures in lung lobes.[42] It is also necessary because there are some low density nodules, which may remain undetected. Hence, it is imperative for us to account for every potential nodule candidate. In this paper, we propose a multi-scale dot enhancing filter,[43] based on Hessian matrix for image enhancement. In the first step, a Gaussian smoothing,[44] on all the corresponding 2D slices is performed to reduce the noise and sensitivity effect. A 2D smoothing is applied because it produces promising results and reduces computational complexity. After Gaussian smoothing, Hessian matrix and its eigen values $|\lambda_2| < |\lambda_1|$ are calculated for every pixel to determine the local shape of the structure.[42] The suspected pulmonary nodule region exhibits the form of a circular or oval object whereas vascular tissue structures presents a line-like elongated structure. Therefore this property can be used to distinguish different shape structures present in lung lobes.[45]

For circular structures we have:

$$\lambda_1 = \lambda_2 << 0 \tag{3}$$

And for Line structures:

$$\lambda_1 << 0,\ \lambda_2 = 0 \tag{4}$$

Here we have assumed that we are trying to enhance bright objects from their dark background. The filter response can be calculated as:

$$E_{circle} = \begin{cases} |\lambda_2|^2 / |\lambda_1|, & \lambda_1 < 0, \lambda_2 < 0 \\ 0, & otherwise \end{cases} \tag{5}$$

Because we have different pulmonary nodule diameters, a single scale for enhancement was not good enough. Therefore, we used multi-scale enhancement filtering to optimize the extraction. By assuming that the nodules to be detected have diameters in the range $[d_o, d_1]$, the N discrete smoothing scales in the range $\left[{}^{d_o}/_{4}, {}^{d_1}/_{4}\right]$ can be computed as:[43]

$$\sigma_1 = \frac{d_0}{4},\ \ \sigma_2 = r\frac{d_0}{4},\ \ \sigma_3 = r^2\frac{d_0}{4},\ \ \ldots\ldots\ldots\ldots\ \sigma_N = r^{N-1}\frac{d_0}{4} = \frac{d_1}{4} \tag{6}$$

where $r = \left(\frac{d_1}{d_o}\right)^{\left(1/(N-1)\right)}$ and each scale has the corresponding nodule diameter 4σ. The algorithm works as follows: First, we determine the specified σ scale of the image by using Eq. (6) and smooth the image using Gaussian function. Initially, smallest value of scale is selected which is incrementally extended. Then the two eigen values of Hessian matrix, λ_1 and λ_2 are calculated which are followed by the calculation of respective value of E_{circle} filter. This process is repeated for different scales and finally we integrate the filter's output values to obtain the maximum value for the best enhanced effect and generate the resultant image as:

$$I_D(x,y) = \begin{cases} 1, & if: E_{circle,max} \\ 0, & otherwise \end{cases} \quad (7)$$

where $E_{circle,max} = max\ \ E_{circle}, \sigma \in [\sigma_{min}, \sigma_{max}]$. Fig. 5 shows the results of image enhancement at different slices. After enhancement, the lung nodule candidates are detected by applying optimal thresholding (explained in section 2.1) on dot enhanced images. Then a rule-based analysis has been made based on some initial measurements like area, diameter and volume whether to keep or discard the detected nodule candidate.[13] The advantage of rule-based analysis is that it eliminates the objects which are too small or too big to be considered a nodule candidate and thus reduces the workload for the next stage. All segmented objects must meet the following basic size requirements to be considered a good nodule candidate. The computed area may lie in the range 4-908 mm^2, equivalent to a diameter 2.5-34 mm and the volume must not exceed the range 8-20580 mm^3. After rule-based analysis, several features are extracted from good nodule candidates and used to train the SVM classifier in the next step.

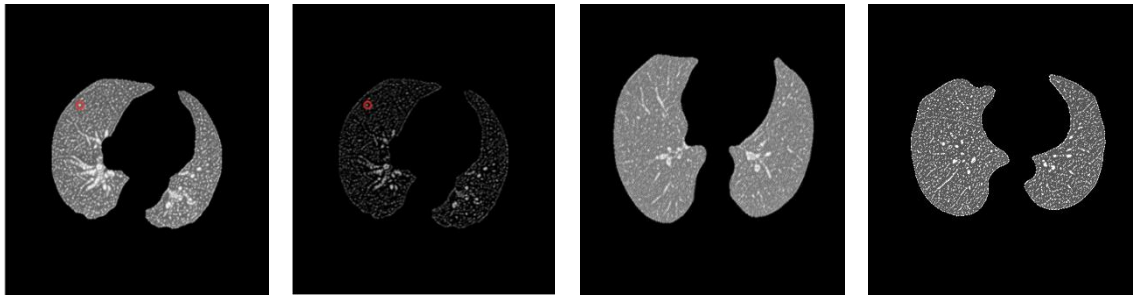

(a) (b) (c) (d)

Fig. 5. Example images showing results of image enhancement at different slices. (a) and (b) shows a low density nodule in red circle, which is detected after image enhancement where (c) and (d) shows the other two slices after image enhancement.

2. C. Lung Nodule Classification

The ultimate goal of this step is to reduce the false positives per scan. It comprises of two steps: feature extraction, and classification. We briefly provide details on each of these steps in the following.

2. C.1. Feature Extraction

Feature extraction can be used to reduce the original dataset to certain characteristics, which can differentiate one input from others. Nodules have their own characteristics, which differentiate them from other anatomical structures present in lung lobes.[9] We have selected an optimum set of lung nodule features, which has been achieved after experimentation and correlation analysis. Correlation coefficient of any two samples *A* and *B* can be calculated as: [46]

$$r_{AB} = \frac{\sum_i (a_i - \bar{a})(b_i - \bar{b})}{\sqrt{\sum_i (a_i - \bar{a})^2 \sum_i (b_i - \bar{b})^2}} \tag{8}$$

where $\bar{a}$ and $\bar{b}$ represents the means of *A* and *B*, respectively. Rigorous experimentation has been done in selection of feature set which gives the optimum results in classification of lung nodule candidates. Our approach was to select a large initial set of features that represents the state of the art in features utilized by the most successful published CAD systems. From this initial pool, we carried out feature selection and trimmed down the feature set to the optimal subset for nodule detection considering both the sensitivity and the FP/scan. We can broadly classify the selected nodule features into: shape, intensity, and texture related quantities as shown in Table 2. These features were extracted from all the lung nodule candidates and used for classification. Examples of some detected nodule candidates can be seen in Fig. 6.

2. C.2. Support Vector Machine Classifier

Once the feature vectors have been formed, they are used as an input for classification and false positive reduction. In our proposed method, we have used SVM classifier as it is computationally efficient and gives better results.[47,48] To train the classifier, we use the annotated data from the radiologists. Normally the number of nodule samples are much less than the number of non-nodules, affecting the performance of a classifier. To remove this biasness, we have balanced our dataset by selecting the equal number of nodules and non-nodules randomly. Next, the balanced dataset is randomly split into training and testing datasets. More specifically, 70% of the data is used for

305 **Table 2 -** Extracted features of nodule candidates.

Shape Features				*Intensity Features*		*Texture Features*	
Area [13]	$A = \sum_{o \in Om} o$	Elongation [9]	$E = \frac{a}{b}$	Mean[39]	$\bar{X} = \frac{\sum_{i=1}^{n} x_i}{n}$	Normalized GLCM [50]	$\hat{P}_\delta(i,j) = \frac{P_\delta(i,j)}{\sum_i^{L-1}\sum_j^{L-1} P_\delta(i,j)}$
Image Moments [7]	$m_{pq} = \sum_x \sum_y x^p y^q f(x,y)$	Perimeter [32]	$L(I) = \sum_{(x,y)\in C} I(x,y)$	Variance [39]	$S^2 = \frac{\sum_{i=1}^{n}(x_i - \bar{x}^2)^2}{n-1}$	Energy[49]	$ene = \sum_{i=0}^{L-1}\sum_{j=0}^{L-1} \hat{P}_\delta^2(i,j)$
Central Moments [7]	$\mu_{pq} = \sum_x \sum_y (x-x_0)^p (y-y_0)^q f(x,y)$	Circularity [32]	$C = \frac{4\pi A}{L^2}$	Maximum Value Inside [13]	$I_{max} = max(I)$	Entropy [50]	$ent = -\sum_{i=0}^{L-1}\sum_{j=0}^{L-1} \hat{P}_\delta(i,j)\log\hat{P}_\delta(i,j)$
Centroid [7]	$x_0 = m_{10}/m_{00}$, $y_0 = m_{01}/m_{00}$	Roundness [32]	$R = \frac{4A}{\pi L^2}$	Minimum Value Inside [13]	$I_{min} = min(I)$	Inverse Difference Moment [50]	$idm = \sum_{i=0}^{L-1}\sum_{j=0}^{L-1} \frac{\hat{P}_\delta(i,j)}{1+(i-j)^2}$
Major Axis Length [14]	$a = 2[\frac{2(\mu_{20}+\mu_{02}+\sqrt{(\mu_{20}-\mu_{02})^2+4\mu_{11}^2})}{\mu_{00}}]^{1/2}$	Volume [9]	$Vol = \sum_{o\in O} o$	Skewness [39]	$Skew = \frac{\sum_{i=1}^{n}(\mathrm{x_i}-\bar{\mathrm{x}})^3}{(\mathrm{n}-1)^3}$	Contrast [50]	$con = \sum_{n=0}^{L-1} n^2 \left\{\sum_{i=0}^{L-1}\sum_{j=0}^{L-1} P_\delta^{\wedge}(i,j)\right\}$
Minor Axis Length[14]	$b = 2[\frac{2(\mu_{20}+\mu_{02}-\sqrt{(\mu_{20}-\mu_{02})^2+4\mu_{11}^2})}{\mu_{00}}]^{1/2}$	Compactness [9]	$Cmp = \frac{Vol}{\frac{4}{3}\pi r^3}$	Kurtosis [39]	$Kurt = \frac{\sum_{i=1}^{n}(\mathrm{x_i}-\bar{\mathrm{x}})^4}{(\mathrm{n}-1)\mathrm{s}^4}$		

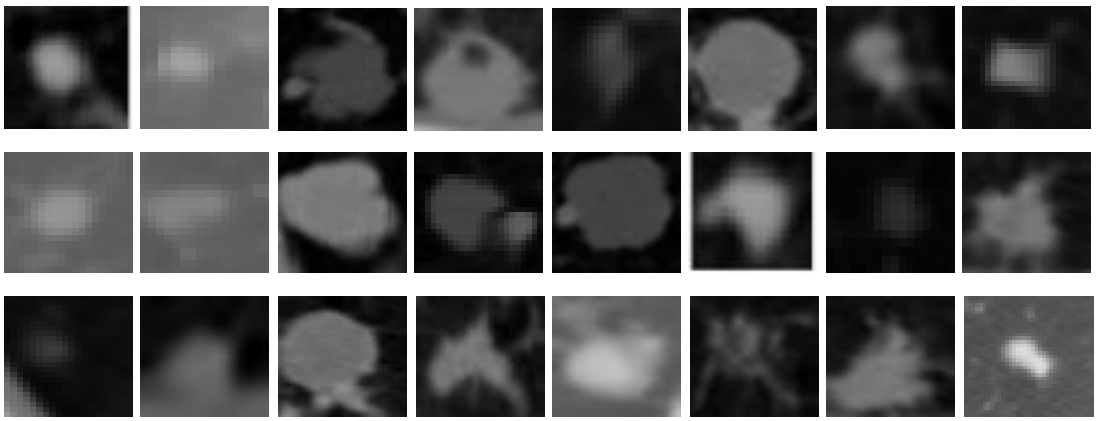

(a)

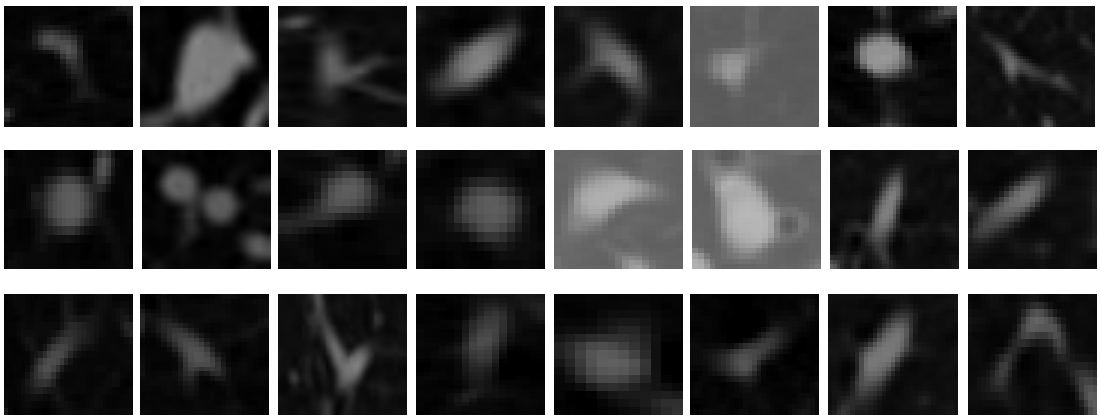

(b)

Fig. 6. Examples of detected candidates (a) nodules (b) non-nodules. It can be seen that nodule diversity and their close resemblance to other anatomic structures present in the lung lobes make the task of detection more challenging and produces false positives, which are being reduced with the aid of a classifier.

training and 30% of the data is held out as a test set for the final evaluation of the system. In training phase, we have used k-fold cross-validation scheme for model selection and validation. In k-fold cross-validation scheme, training data set is randomly divided into k-equal sized sub-samples. Then from those samples, one sample is selected as validation data for model assessment and remaining k-1 samples are used for training the classifier. This process is repeated k-times. The k results from the folds are then averaged to produce a single estimation. The advantage of this scheme is that each sample is used for training and validation purposes having each value used only once for validation. In training phase, the input to the classifier consists of the feature vector and the known class labels. The SVM solves the following optimization problem:

$$\min_{\omega,\varepsilon,b}\left\{\frac{1}{2}w^T w + C\sum_{i=1}^{n}\varepsilon_i\right\} \tag{9}$$

Subject to (for any i=1 ...N)

$$f(x_i) = y_i(w^T \emptyset(x_i) - b) \geq 1 - \varepsilon_i \quad (10)$$

Where $\varepsilon_i \geq 0$ and $f(x_i)$ is the decision function. C >0 can be defined as penalty parameter of the error term. In addition, SVM can efficiently perform non-linear classification using kernel trick.[47] In this paper, we have used a polynomial and a radial basis function as kernel functions as follows:

$$K(x_i, x_j) = \exp\left(-\gamma \|x_i - x_j\|^2\right) \quad (11)$$

$$K(x_i, x_j) = (\gamma x_i^T x_j + r)^d \quad (12)$$

Where γ, r and d are kernel parameters. The penalty factor and kernel scale parameters have been optimized using grid search. An exhaustive grid search has been used to select these parameters where the range of penalty factor and kernel is selected as C = 10^0, ……, 10^2 and γ = 2^{-3}, …… , 2^3 respectively. The interval between the two consecutive values of penalty factor and kernel is set as 1 and 0.2 respectively. Different pair of (C, γ) values are tried and the one with best cross-validation accuracy is picked.[51,52] This optimized pair of parameter is then used to train the classifier using only training data.

Once the classifier is trained and its hyper-parameters are tuned, then the final evaluation of the classifier is done using the test set only. More specifically, 30% of the data held out initially is used for final evaluation of the classifier and the corresponding results are reported in next section. One thing to note that now the input to the classifier consists of only the feature vector.

Feature selection was done using the training set only. Once we get the optimal feature set for nodule detection considering both the sensitivity and the FP/scan from training dataset, then we fix it and apply it to the test set.

The performance of a classifier can be calculated by the standard performance metrics mainly sensitivity, specificity, accuracy and receiver operating characteristic curves (ROC curves).[53] ROC curves are obtained by plotting the sensitivity and false positive rate for different threshold values. The area under the ROC curves summarizes the performance of the classifier. These metrics can be calculated as follows:

$$sensitivity = \frac{TP}{TP + FN} \quad (13)$$

$$specificity = \frac{TN}{TN + FP} \quad (14)$$

$$accuracy = \frac{TP + TN}{TP + FP + TN + FN} \quad (15)$$

Where TP, TN, FP, and FN denote true positive, negative, and false positive and negative labels.

3. RESULTS AND DISCUSSION

We have done an extensive evaluation of our proposed system on Lung Image Database Consortium (LIDC). LIDC is a publicly available database accessible from The Cancer Imaging Archive (TCIA). We have considered the 850 scans[1] (LIDC-IDRI-0001 to LIDC-IDRI-0844) of this dataset, which contains nodules of size 3-30 mm fully annotated by four expert radiologist in two consecutive sessions. Each CT scan consists of 150-300 slices where each slice is of size 512*512 and 4096 gray level values in HU. The pixel spacing is 0.78 mm – 1 mm and reconstruction interval varies from 1-3 mm.

We have considered all the nodules (even if only one of the radiologists has marked it) in evaluation of our proposed system. The total number of nodules in 850 CT scans is 2242. In our evaluation, we have considered each detected nodule as a nodule if its distance to any of the nodule in the dataset is smaller than 1.5 times the radius of that nodule. This value is achieved by experiments and we call it near hit. If a hit has been made on a detected nodule we call it as true positive otherwise it is called false positive.

Our system detects 2112 nodules with 38682 non-nodules, which gives the detection rate of 94.20 % with 45.51 % FP/scan. Note that these non-nodules have been further reduced by the use of a classifier at the classification stage. Results have been summarized in the following tables. Table. 3 shows the classification results of SVM with different kernel functions on test dataset while using 2, 5 and 7-fold cross validation schemes in training phase. It is to note that penalty factor and kernel parameters of these models have been optimized using grid search. For SVM-Gaussian, the pair (C=1 and γ= 0.125) achieved maximum cross-validation accuracy and was used to train the model while for SVM-Cubic, the pair (C=11 and γ= 1.325) achieved maximum cross-validation accuracy and was used to train the model. Lastly, for SVM-Quadratic, the pair (C=9 and γ= 0.525) achieving maximum cross-validation accuracy was selected to train the model. Our system has achieved a sensitivity of 98.41 % and an accuracy of 97.40 % using SVM with Gaussian kernel function. It can be seen that Gaussian kernel function outperforms other kernel functions regarding the accuracy of the system and 7-fold cross

[1] The case no. LIDC-IDRI-0132,0151,0315,0332,0355,0365,0442,0484 appear twice as distinct cases in the dataset and cases with IDs. LIDC-IDRI-0238,0585 do not exist in the dataset.

validation scheme yields the maximum accuracy. The performance of the system with Gaussian kernel function remains almost the same in 2 and 5-fold cross validation schemes with a slight difference in metrics. Other two kernel functions, SVM-Cubic and Quadratic achieve the highest sensitivities of 92.67 % and 80.90 % respectively.

In addition to performing grid search for the selection of (C, γ), we have also experimented with different values of kernel scale and penalty factor while keeping one of them constant to observe the effect of these parameters. Table. 4 shows the classification results of SVM-Gaussian using different kernel scale values in 2-fold cross validation scheme. We have evaluated our system using different values of kernel scale between the range 0.3 to 3. The penalty parameter has been kept constant with a value of 1. It can be seen that the performance of the system decreases with the increasing value of scale after achieving the maximum accuracy at initial value of γ=0.3. The system achieves a lowest accuracy of 83.30 % for a value of γ=3. Table. 5 shows the classification results of SVM-Gaussian using different penalty parameter values in 2-fold cross validation scheme. The value of the penalty parameter used varies from 1 to 4. The value of kernel scale has been kept constant. It can be seen that the accuracy of the system increases with the increasing value of penalty parameter and attains a maximum value of 97.0 % for *C*=4.

In addition to the SVM classifier, we have also evaluated our system using some other supervised classifiers mainly K-Nearest-Neighbour, Decision Tree, Linear Discriminant and Boosted Tree. Table. 6 shows the classification results of these classifiers using 2-fold cross validation scheme. It can be seen that *Decision Tree* shows better performance as compared to other classifiers by achieving maximum accuracy and sensitivity while *Linear Discriminant* performs poorly by achieving the lowest sensitivity.

From the review of the existing methods, we found that it is very hard to compare the results with the previously published work because of their use of non-uniform performance metrics and different evaluation criteria including the dataset and types of nodules considered. Despite of this constraint, we have tried to make a performance comparison of our proposed system with the other Lung CAD systems as shown in Table. 7. It can be seen that our proposed system shows better performance as compared to other systems regarding sensitivity and FP/scan. Other systems which are close in the performance are Choi *et al.*[3], Messay *et al.*[13] and Akram *et al.*[39]. Choi *et al.*[3] proposed a novel shape-based feature extraction method. Eigen value decomposition of Hessian matrix was done to obtain the surface elements which could describe the local shape information of the target object and features were formed from these surface elements. The system was evaluated by considering 148 nodules in 84 scans of LIDC dataset. System shows good performance in terms of sensitivity by achieving a value of 97.5 %

but underperforms in terms of false positives by having a value of 6.76 FP/ scan. Messay *et al.*[13] computed a detailed feature set consisting of 245 features (2D & 3D) mainly belonging to feature classes of shape, intensity and gradient. A sequential forward selection method was next applied to obtain the optimum feature subset. The system was evaluated using LIDC dataset and considering 143 nodules. System shows good performance in terms of false positives with a value of 3 FP/scan but underperforms in terms of sensitivity. Akram *et al.* [39] computed the 2D shape features (Area, Diameter, Perimeter, Circularity), 3D shape features (Volume, Compactness, Bounding Box Dimensions, Elongation, Principal Axis Length) and 2D and 3D intensity based statistical features (Mean inside, Mean outside, Variance inside, Kurtosis inside, Skewness inside, Minimum value inside, Eigen values). The system was evaluated using LIDC dataset. System shows good sensitivity having a value of 95.31 % but the number of nodules used to validate the results is too small.

3. A. Feature Ranking

Various features have been proposed in literature to differentiate between nodules and other anatomical structures but the research on measuring the effectiveness of these features have been limited. In this paper, we have compared different classes of features to determine the most relevant feature class. Table. 8 shows the classification results of SVM-Gaussian using different classes of features in 2-fold cross validation scheme. Features from class *Shape* shows the maximum performance regarding sensitivity and accuracy of the system as compared to other feature classes. But results clearly show that it is very difficult to achieve high performance metrics using only a single class therefore hybrid approach in feature selection remains a better choice.

Table 3 - Classification Results of SVM on test dataset with different kernel functions using 2, 5 and 7-fold Cross Validation Scheme in training phase.

k-fold	Classifier	AUC	Accuracy (%)	Sensitivity (%)	Specificity (%)	FPs/Scan
2-Fold	SVM-Gaussian	0.995011	97.10	98.15	96.01	2.19
	SVM-Cubic	0.942661	90.10	92.12	88.63	3.50
	SVM-Quadratic	0.906624	83.40	80.21	85.73	4.27
5-Fold	SVM-Gaussian	0.995264	97.40	98.32	96.46	1.88
	SVM-Cubic	0.949235	90.10	92.28	88.31	3.36
	SVM-Quadratic	0.916236	83.80	80.90	86.16	3.98
7-Fold	SVM-Gaussian	0.994015	97.40	98.41	96.40	1.91
	SVM-Cubic	0.955405	90.90	92.67	89.38	3.11
	SVM-Quadratic	0.919643	83.20	80.29	85.59	3.76

Table 4 - Classification Results of SVM-Gaussian on test dataset using different γ values and 2-fold Cross Validation Scheme in training phase.

Penalty Parameter (C)	Kernel scale (γ)	AUC	Accuracy (%)	Sensitivity (%)	Specificity (%)	FPs/scan
1	**0.3**	0.994214	97.00	98.04	95.87	1.31
1	**0.5**	0.992096	96.80	97.92	95.53	1.56
1	**1**	0.988753	96.40	97.86	95.26	1.79
1	**1.3**	0.973747	93.30	94.12	92.67	2.00
1	**1.5**	0.964420	91.20	91.14	91.34	2.36
1	**1.8**	0.950276	88.70	86.63	90.40	2.62
1	**2**	0.941655	87.40	84.79	89.57	2.85
1	**2.5**	0.922157	84.30	79.98	87.93	3.29
1	**3**	0.913129	83.30	79.60	86.41	3.71

425

Table 5 - Classification Results of SVM-Gaussian on test dataset using different C values and 2-fold Cross Validation Scheme in training phase.

Penalty Parameter (C)	Kernel scale (γ)	AUC	Accuracy (%)	Sensitivity (%)	Specificity (%)	FPs/scan
1	1	0.988753	96.40	97.86	95.26	1.79
2	1	0.991408	96.70	98.12	95.45	1.74
3	1	0.991548	96.90	98.23	95.07	1.84
4	1	0.992020	97.00	98.32	95.26	1.79

Table 6 - Classification Results of different classifiers on test dataset using 2-fold Cross Validation Scheme in training phase.

Classifier	AUC	Accuracy (%)	Sensitivity (%)	Specificity (%)	FPs/scan
Decision Tree	0.941685	91.40	96.03	87.55	3.39
Linear Discriminant	0.792127	74.10	57.06	88.18	3.25
K-Nearest-Neighbour	0.882561	78.40	83.04	74.59	6.93
Boosted Tree-Ensemble	0.959660	89.60	91.67	87.93	3.29

430

Table 7 - Performance Comparison of Different CAD Systems, *N/A means Not Available.

CAD Systems	Year	Data Set	Nodule Size(mm)	Number of Nodules	Sensitivity (%)	FPs/scan
Proposed System	2016	LIDC	3-30	2242	98.15	2.19
Akram *et al.*[39]	2016	LIDC	3-30	50	95.31	N/A
Choi *et al.*[3]	2014	LIDC	3-30	148	97.50	6.76
Teramoto *et al.*[35]	2014	Private	4-30	103	83.00	5.00
Choi *et al.*[9]	2013	LIDC	3-30	151	95.28	2.27

Tartar *et al.*[32]	2013	Private	2-20	95	89.60	7.90
Orozco *et al.*[31]	2013	LIDC,ELCAP	2-30	75	84.00	7.00
Assefa *et al.*[37]	2013	ELCAP	N/A	165	81.00	35.15
Choi *et al.*[14]	2012	LIDC	3-30	76	94.10	5.45
Messay *et al.*[13]	2010	LIDC	3-30	143	82.66	3.00
Sousa *et al.*[29]	2010	Private	3-40	33	84.84	N/A

Table 8 - Classification Results of SVM-Gaussian on test dataset using different feature classes and 2-fold Cross Validation Scheme in training phase.

Features	AUC	Accuracy (%)	Sensitivity (%)	Specificity (%)	FPs/scan
Intensity	0.780086	72.40	68.53	76.49	6.13
Shape	0.901880	84.60	80.59	87.87	3.62
Texture	0.835350	76.40	71.89	80.09	5.43

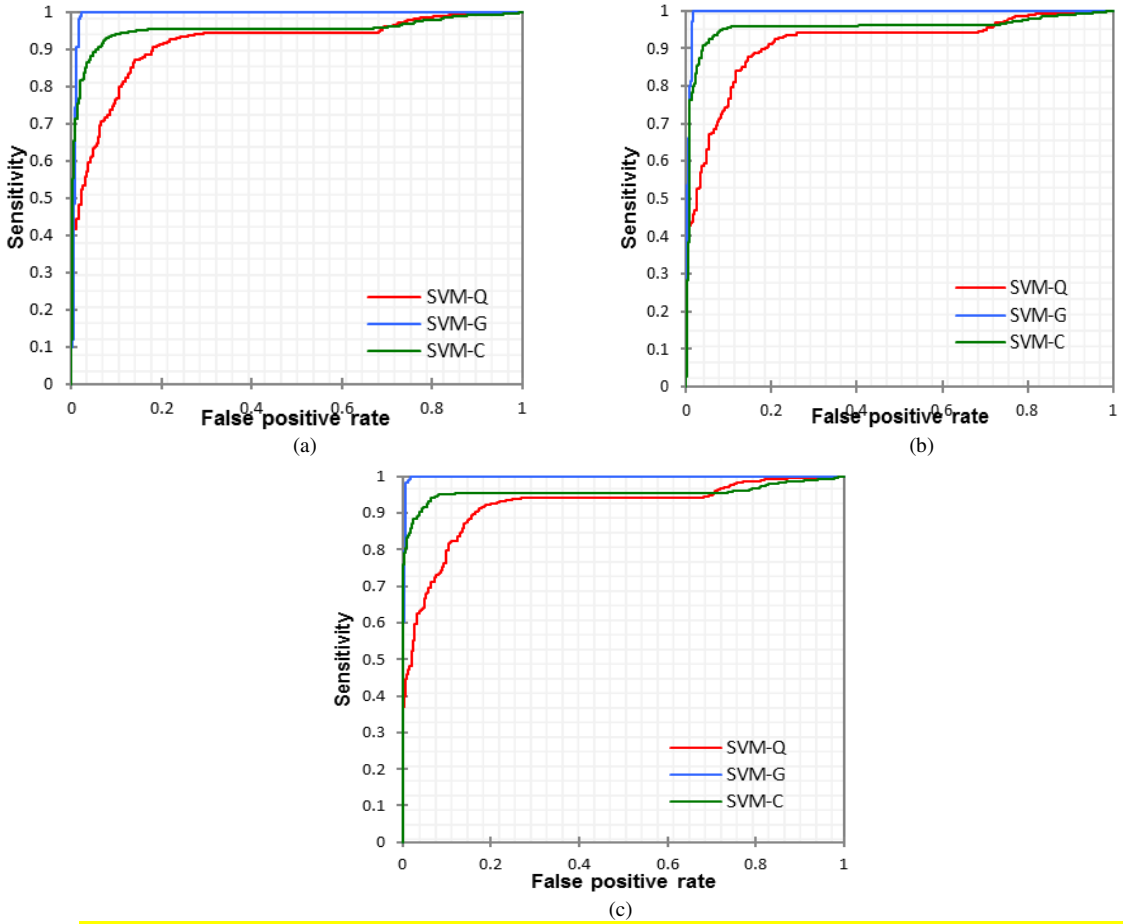

Fig. 7. ROC curves of the SVM classifier with different kernel function using (a) 2-Fold Scheme, (b) 5-Fold Scheme (c) 7-Fold Scheme SVM-Q: Quadratic kernel function, SVM-G: Gaussian kernel function, SVM-C: Cubic kernel function.

ROCs curves have been drawn to visualize the classifier's performance. Fig. 7 shows the ROCs curves for SVM classifier with different kernel functions using 2, 5 and 7-fold cross validation scheme, respectively. It can be seen

that SVM Gaussian kernel function outperforms the other two kernel functions while SVM Quadratic function shows the lowest performance. Fig. 8 (a) shows the ROCs curves for SVM classifier with Gaussian kernel function using different kernel scale values in 2-fold cross validation scheme.

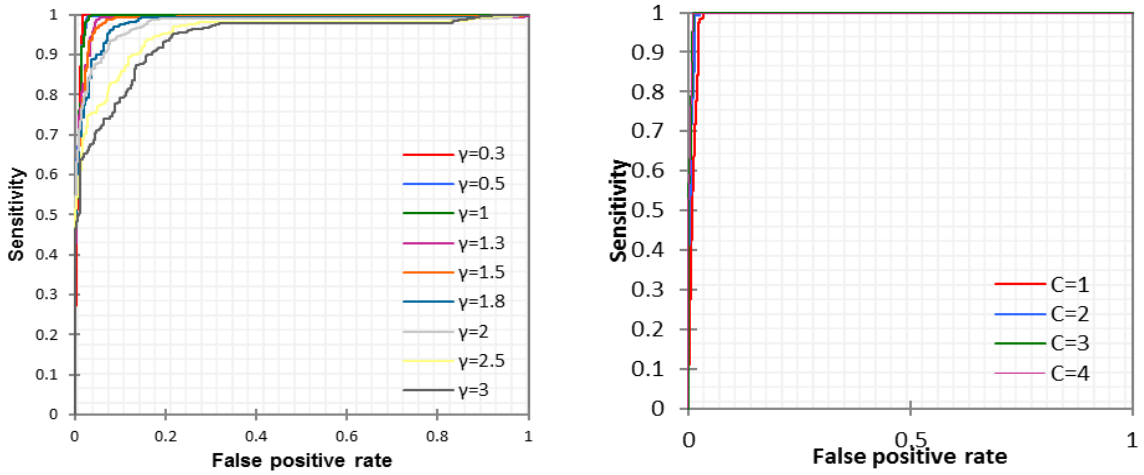

(a) (b)

Fig. 8. ROC curves of the SVM classifier with Gaussian kernel function using 2-Fold cross validation scheme with (a) different kernel scale γ values, varying from 0.3 to 3 (b) with different penalty parameter C values varying from 1 to 4.

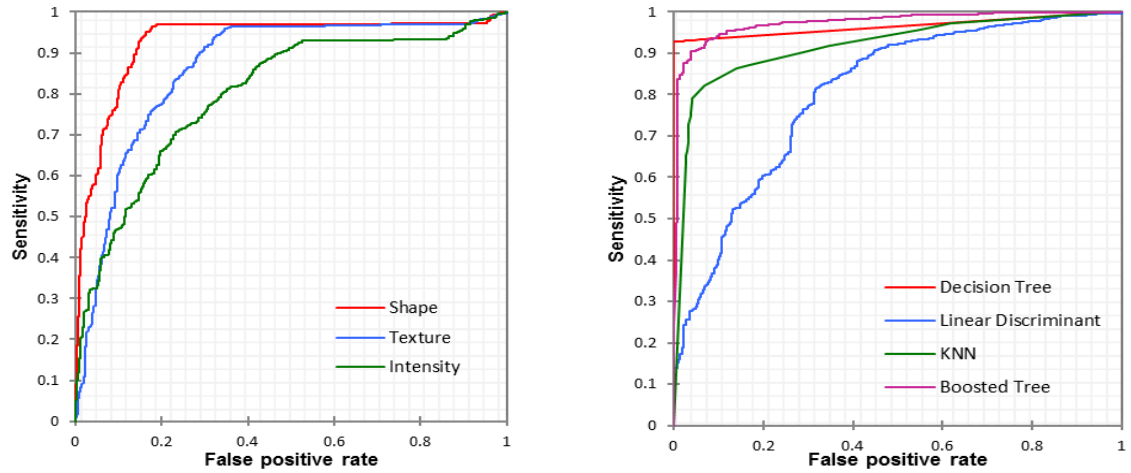

(a) (b)

Fig. 9. (a) ROC curves of SVM classifier with Gaussian kernel function using 2-Fold cross validation scheme with different feature classes (b) ROC curves of different classifiers using 2-Fold cross validation scheme.

The kernel scale value varies from 0.3 to 3 by keeping the penalty parameter constant. It can be seen that the performance of the classifier decreases with the increasing value of γ. Fig. 8 (b) shows the ROCs curves for SVM classifier with Gaussian kernel function using different penalty parameter values in 2-fold cross validation scheme. The penalty parameter value varies from 1 to 4 by keeping the kernel scale value constant. It can be seen that the performance of the classifier remains almost the same with minor increase. Fig. 9 (a) shows the ROCs

curves for different feature classes using SVM classifier with Gaussian kernel function in 2-fold cross validation scheme. It can be seen that features from class *Shape* shows the maximum performance as compared to other two feature classes. Fig. 9 (b) shows the ROCs curves for different classifiers in 2-fold cross validation scheme. It is noteworthy that *Linear Discriminant* classifier performs poorly as compared to other classifiers by having the lowest area under the curve. Fig. 10 shows the overall performance of our proposed CAD system by the free-response ROC (FROC) curves [54] using SVM classifier with different kernel functions and 2-fold cross validation scheme. The system shows robust and accurate performance in detecting nodules.

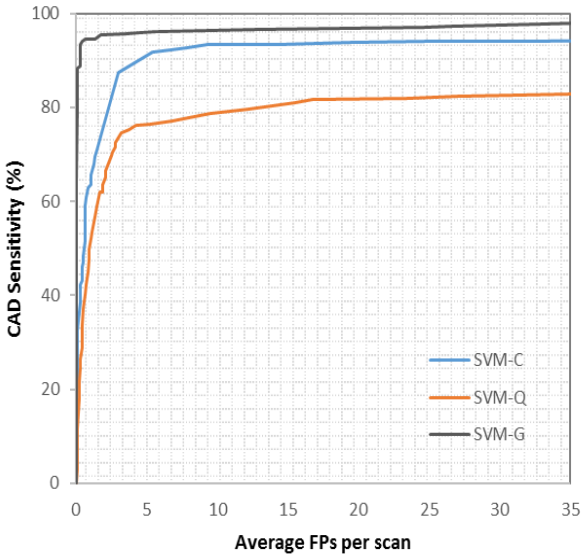

Fig. 10. FROC curves of the proposed system with respect to the different kernel functions of SVM classifier.

4. CONCLUSION

A well performing CAD system contribute to the health provision by helping the expert radiologist in the detection of lung cancer and by providing them with a second opinion. In this paper, we have proposed a method with hybrid feature set for lung nodule detection. In the pre-processing stage, the lung image has been thresholded using optimal thresholding, followed by background removal, hole filling operations and lung segmentation. Then the contour correction of the segmented lung fields has been made to include juxta-pleural nodules. The candidate nodules have been detected and segmented simultaneously from an enhanced image using multi scale dot enhancement filter. Shape, intensity and texture features have been extracted from lung nodule candidates and used for false positive reduction using a SVM classifier. The proposed system has been evaluated using the LIDC dataset and k-fold cross validation. The achieved sensitivity is 98.15 % with 2.19 false positive per scan only.

In this paper, we have used a hybrid feature set to improve the classification accuracy of the system. Moreover,

we have also made a comparison of feature classes which clearly indicate that no single feature can detect the nodules with high precision. Thus, choosing right set of features can improve the overall accuracy of the system by improving the sensitivity and reducing false positives. We also experimented with different classifiers to assess the performance of the system but results clearly show that SVM, with the flexibility of having different kernel functions, remains a better choice as compared to other classifiers in terms of accuracy.

A future area which needs to be focused is the detection of micro nodules (< 3mm). Future CAD systems should be able to detect all types of nodules (including micro nodules) while maintaining the same precision in terms of sensitivity and reduced number of false positives per scan. Moreover, the systems should be evaluated on large datasets to achieve more robustness.

CONFLICT OF INTEREST DISCLOSURE

The authors declare that there is no conflict of interest.

REFERENCES

[1] R. Siegel, K. Miller, and A. Jemal, "Cancer statistics , 2015 .," CA Cancer J Clin **65**(1), 29 (2015).

[2] J.M. Diaz, R.C. Pinon, and G. Solano, "Lung cancer classification using genetic algorithm to optimize prediction models," in *IISA 2014, 5th Int. Conf. Information, Intell. Syst. Appl.*(IEEE, 2014), pp. 1–6.

[3] W.J. Choi and T.S. Choi, "Automated pulmonary nodule detection based on three-dimensional shape-based feature descriptor," Comput. Methods Programs Biomed. **113**(1), 37–54 (2014).

[4] I.R.S. Valente, P.C. Cortez, E.C. Neto, J.M. Soares, V.H.C. de Albuquerque, and J.M.R.S. Tavares, "Automatic 3D pulmonary nodule detection in CT images: A survey," Comput. Methods Programs Biomed. **124**, 91–107 (2015).

[5] W.J. Kostis, A.P. Reeves, D.F. Yankelevitz, and C.I. Henschke, "Three-Dimensional Segmentation and Growth-Rate Estimation of Small Pulmonary Nodules in Helical CT Images," IEEE Trans. Med. Imaging **22**(10), 1259–1274 (2003).

[6] S.S. Parveen and C. Kavitha, "A Review on Computer Aided Detection and Diagnosis of lung cancer nodules," Int. J. Comput. Technol. **3**(3), 393–400 (2012).

[7] M. Mabrouk, A. Karrar, and A. Sharawy, "Computer Aided Detection of Large Lung Nodules using Chest Computer Tomography Images," Computer (Long. Beach. Calif). **3**(9), 12–18 (2012).

[8] S.K. Vijai Anand, "Segmentation coupled textural feature classification for lung tumor prediction," in *2010 Int. Conf. Commun. Control Comput. Technol.*(IEEE, 2010), pp. 518–524.

[9] W.J. Choi and T.S. Choi, "Automated pulmonary nodule detection system in computed tomography images: A hierarchical block classification approach," Entropy **15**(2), 507–523 (2013).

[10] S.G. Armato *et al.*, "The Lung Image Database Consortium (LIDC) and Image Database Resource Initiative (IDRI): a completed reference database of lung nodules on CT scans.," Med. Phys. **38**(2), 915–931 (2011).

[11] C.I. Henschke *et al.*, "Early lung cancer action project: a summary of the findings on baseline screening.," Oncologist **6**(2), 147–52 (2001).

[12] Public Lung Image database to address drug response. Vision and Image Analysis Group (VIA) and International Early Lung Cancer Action Program (I-ELCAP) Labs, Cornell University. http://www.via.cornell.edu/crpf.html; 2008 [accessed 24-04-16].

[13] T. Messay, R.C. Hardie, and S.K. Rogers, "A new computationally efficient CAD system for pulmonary nodule detection in CT imagery," Med. Image Anal. **14**(3), 390–406 (2010).

[14] W.J. Choi and T.S. Choi, "Genetic programming-based feature transform and classification for the automatic detection of pulmonary nodules on computed tomography images," Inf. Sci. (Ny). **212**, 57–78 (2012).

[15] J. Dehmeshki, X. Ye, X. Lin, M. Valdivieso, and H. Amin, "Automated detection of lung nodules in CT images using shape-based genetic algorithm," Comput. Med. Imaging Graph. **31**(6), 408–417 (2007).

[16] J.J. Suárez-Cuenca *et al.*, "Application of the iris filter for automatic detection of pulmonary nodules on computed tomography images," Comput. Biol. Med. **39**(10), 921–933 (2009).

[17] X. Ye *et al.*, "Shape based computer-aided detection of lung nodules in thoracic CT images," IEEE Trans. Biomed. Eng. **56**(7), 1810–1820 (2009).

[18] I. Sluimer, M. Prokop, and B. van Ginneken, "Toward automated segmentation of the pathological lung in CT," Med. Imaging, IEEE. **24**(8), 1025–1038 (2005).

[19] G. De Nunzio *et al.*, "Automatic lung segmentation in CT images with accurate handling of the hilar region," J. Digit. Imaging **24**(1), 11–27 (2011).

[20] A.M. Ali and A.A. Farag, "Automatic Lung Segmentation of Volumetric Low-Dose CT Scans Using Graph Cuts," in *Adv. Vis. Comput. Pt I, Proc.*(Springer Berlin Heidelberg, 2008), pp. 258–267.

[21] E. van Rikxoort, B. de Hoop, and M. Viergever, "Automatic lung segmentation from thoracic computed tomography scans using a hybrid approach with error detection," Med. Phys. **36**(7), 2934 (2009).

[22] D.S. Paik *et al.*, "Surface normal overlap: a computer-aided detection algorithm with application to colonic polyps and lung nodules in helical CT," Med. Imaging, IEEE Trans. **23**(6), 661–675 (2004).

[23] J. Jiantao Pu *et al.*, "Shape 'break-and-repair' strategy and its application to automated medical image segmentation.," IEEE Trans. Vis. Comput. Graph. **17**(1), 115–24 (2011).

[24] T. Kubota, A.K. Jerebko, M. Dewan, M. Salganicoff, and A. Krishnan, "Segmentation of pulmonary nodules of various densities with morphological approaches and convexity models," Med. Image Anal. **15**(1), 133–154 (2011).

[25] S.L.A. Lee, A.Z. Kouzani, and E.J. Hu, "Random forest based lung nodule classification aided by clustering," Comput. Med. Imaging Graph. **34**(7), 535–542 (2010).

[26] M. Niemeijer, M. Loog, M.D. Abràmoff, M.A. Viergever, M. Prokop, and B. van Ginneken, "On Combining Computer-Aided Detection Systems," IEEE Trans. Med. Imaging **30**(2), 215–223 (2011).

[27] P.G. Espejo, S. Ventura, and F. Herrera, "A Survey on the Application of Genetic Programming to Classifcation," Ieee Trans. Syst. Man, Cybern. Part C Appl. Rev. **40**(2), 121–144 (2010).

[28] W. Guo, Y. Wei, H. Zhou, and D. Xue, "An adaptive lung nodule detection algorithm," Chinese Control Decis. Conf., IEEE, 2361–2365 (2009).

[29] J.R.F.D.S. Sousa, A.C. Silva, A.C. de Paiva, and R.A. Nunes, "Methodology for automatic detection of lung nodules in computerized tomography images.," Comput. Methods Programs Biomed. **98**(1), 1–14 (2010).

[30] Y. Liu, J. Yang, D. Zhao, and J. Liu, "Computer aided detection of lung nodules based on voxel analysis utilizing support vector machines," FBIE 2009 - 2009 Int. Conf. Futur. Biomed. Inf. Eng. 90–93 (2009).

[31] H.M. Orozco, O.O.V. Villegas, H.D.J.O. Dominguez, and V.G.C. Sanchez, "Lung Nodule Classification in CT Thorax Images Using Support Vector Machines," 2013 12th Mex. Int. Conf. Artif. Intell. 277–283 (2013).

[32] A. Tartar, N. Kilic, and A. Akan, "Classification of pulmonary nodules by using hybrid features," Comput. Math. Methods Med. **2013**, 1–11 (2013).

[33] K. Murphy, B. van Ginneken, A.M.R. Schilham, B.J. de Hoop, H.A. Gietema, and M. Prokop, "A large-scale evaluation of automatic pulmonary nodule detection in chest CT using local image features and k-nearest-neighbour classification," Med. Image Anal. **13**(5), 757–770 (2009).

[34] A. Retico *et al.*, "Pleural nodule identification in low-dose and thin-slice lung computed tomography," Comput. Biol. Med. **39**(12), 1137–1144 (2009).

[35] A. Teramoto *et al.*, "Hybrid method for the detection of pulmonary nodules using positron emission tomography/computed tomography: A preliminary study," Int. J. Comput. Assist. Radiol. Surg. **9**(1), 59–69 (2014).

[36] S. Ozekes and O. Osman, "Computerized lung nodule detection using 3D Feature extraction and learning based

algorithms," J. Med. Syst. **34**(2), 185–194 (2010).

[37] M. Assefa, I. Faye, A.S. Malik, and M. Shoaib, "Lung nodule detection using multi-resolution analysis," 2013 ICME Int. Conf. Complex Med. Eng. 457–461 (2013).

[38] A. Tariq, M.U. Akram, and M.Y. Javed, "Lung nodule detection in CT images using neuro fuzzy classifier," 2013 Fourth Int. Work. Comput. Intell. Med. Imaging 49–53 (2013).

[39] S. Akram, M.Y. Javed, M.U. Akram, U. Qamar, and A. Hassan, "Pulmonary Nodules Detection and Classification Using Hybrid Features from Computerized Tomographic Images," J. Med. Imaging Heal. Informatics **6**(1), 252–259 (2016).

[40] S. Hu, E.A. Hoffman, and J.M. Reinhardt, "Automatic lung segmentation for accurate quantitation of volumetric X-ray CT images," IEEE Trans. Med. Imaging **20**(6), 490–498 (2001).

[41] S.G. Armato, M.L. Giger, C.J. Moran, J.T. Blackburn, K. Doi, and H. MacMahon, "Computerized Detection of Pulmonary Nodules on CT Scans1," RadioGraphics **19**(5), 1303–1311 (1999).

[42] Shi Z, Zhao M, Wang Y, He L, Suzuki K, Jin C, *et al.*, "Hessian-log: A novel dot enhancement filter," ICIC Express Lett. Part B Appl. **6**(8), 1987–1992 (2012).

[43] Q. Li, S. Sone, and K. Doi, "Selective enhancement filters for nodules, vessels, and airway walls in two- and three-dimensional CT scans.," Med. Phys. **30**(8), 2040–2051 (2003).

[44] L. Shapiro and G. Stockman, "Computer Vision," in (Prentice Hall, 2001), p. 580.

[45] Y. Yu and H. Zhao, "Enhancement Filter for Computer-Aided Detection of Pulmonary Nodules on Thoracic CT images," Sixth Int. Conf. Intell. Syst. Des. Appl. **2**, 1200–1205 (2006).

[46] J.L. Rodgers and W.A. Nicewander, "Thirteen Ways to Look at the Correlation Coefficient," Am. Stat. **42**(1), 59 (1988).

[47] B.E. Boser, I.M. Guyon, and V.N. Vapnik, "A training algorithm for optimal margin classifiers," in *Proc. fifth Annu. Work. Comput. Learn. theory - COLT '92*(ACM Press, New York, New York, USA, 1992), pp. 144–152.

[48] T. Sun *et al.*, "Comparative evaluation of support vector machines for computer aided diagnosis of lung cancer in CT based on a multi-dimensional data set," Comput. Methods Programs Biomed. **111**(2), 519–524 (2013).

[49] G.M. Xian, "An identification method of malignant and benign liver tumors from ultrasonography based on GLCM texture features and fuzzy SVM," Expert Syst. Appl. **37**(10), 6737–6741 (2010).

[50] R.M. Haralick, K. Shanmugam, and I. Dinstein, "Textural Features for Image Classification," IEEE Trans. Syst. Man. Cybern. **3**(6), 610–621 (1973).

[51] Chih-Wei Hsu, Chih-Chung Chang, and C.-J.L. "A Practical Guide to Support Vector Classification," Tech. Rep., Taipei, 1–16 (2003).

[52] O. Chapelle and A. Zien, "Semi-Supervised Classification by Low Density Separation," *AISTATS*. **2005**, 57–64 (2005).

[53] J.A. Swets, "Measuring the accuracy of diagnostic systems.," Science **240**(4857), 1285–93 (1988).

[54] D.P. Chakraborty, "Maximum likelihood analysis of free-response receiver operating characteristic (FROC) data," Med. Phys. **16**(4), 561–568 (1989).